Materials Science, *Vol. 21*, *No. 3*, *2003*

Wavelet shrinkage-based noise reduction from the high resolution X-ray images of epitaxial layers

JANUSZ KOZŁOWSKI[1*], JAROSŁAW SERAFIŃCZUK[1], ANDRZEJ KOZIK[2]

[1]Faculty of Microsystem Electronics and Photonics, Wrocław University of Technology, Wybrzeże Wyspiańskiego 27, 50-370 Wrocław, Poland

[2]Institute of Engineering Cybernetics, Wrocław University of Technology, Wybrzeże Wyspiańskiego 27, 50-370 Wrocław, Poland

This paper presents advantages of employing the wavelet method in X-ray high-resolution image analysis of nanostructures. It is shown that many more details of the structure examined can be distinguished in rocking curves (RC) as well as in reciprocal space maps (RSM) after application of the numerical procedure. The method proposed seems to be particularly suitable for imperfect epitaxial layers having significant lattice mismatch with respect to substrate. By means of the wavelet analysis of the X-ray images using de-noising procedure details invisible in raw pictures can be detected such as thickness fringes, gradient of lattice parameters etc., and duration of measurements can be shortened.

Key words: *wavelet, X-ray; epitaxial layer*

1. Introduction

The wavelet method has been widely applied in several signal analyses, e.g. human speech, seismic tremors, engine vibrations, and medical images. All types of signals have to be efficiently encoded, described and modelled. For the first time, the method is applied to X-ray high-resolution image analysis of optoelectronic structures. It seems to be very promising in the case of noised X-ray diffractometric images that are typical of the epitaxial layers having a large lattice mismatch with respect to substrate. In these cases, a diffuse scattering appears, obscuring the readability of the X-ray image.

[*]Corresponding author, e-mail: janusz.kozlowski@ pwr.wroc.pl.

2. Brief introduction to wavelets

Wavelets are a family of basis functions that can be used to approximate other functions by expansion in orthonormal series. They combine such powerful properties as orthonormality, compact support, varying degrees of smoothness, localization both in time and scale (frequency), and fast implementation. One of the key advantages of wavelets is their ability to spatially adapt to features of a function such as discontinuities and varying frequency behaviour. In statistics, the interest in wavelets arose after Daubechies [1] and Mallat [2] connected the wavelets with discrete data processing, and when Donoho and Johnstone [3] showed that wavelet shrinkage has desirable statistical optimality properties in problems connected with reduction of noise. We present here a brief overview to the orthogonal discrete wavelet transformation (DWT) and wavelet shrinkage techniques. For detailed review of the subject we direct the reader to Daubechies [4] and Nason [5].

2.1. Discrete wavelet transformation

Let the function $f(x)$ be sampled at N equally spaced points. In addition, let $f = \big(f(1), f(2), \ldots, f(N)\big) = \big(f_1, \ldots, f_N\big)$ be an element of the Hilbert space $\ell_2(N)$ of all square sum able sequences of the length N.

Let us define **H** and **G** operators $\ell_2(2M) \to \ell_2(M)$ coordinate-wise via

$$a \notin \ell_2(2M) \quad (Ha)_k = \sum_m h_{m-2k} a_m$$
$$(Ga)_k = \sum_m g_{m-2k} a_m$$

These operators correspond to lowpass (**H**) and highpass (**G**) filtering (convolution) followed by downsampling (throwing away every other sample). The inverse process (signal reconstruction) is possible, since for quadrature mirror filters $\{h_k\}$ and $\{g_k\}$ the perfect reconstruction conditions are satisfied:

$$\mathbf{H}\mathbf{G}^* = \mathbf{G}\mathbf{H}^* = 0, \qquad \mathbf{H}^*\mathbf{H} + \mathbf{G}^*\mathbf{G} = \mathbf{I}$$

where $\mathbf{H}^*$ and $\mathbf{G}^*$ are adjoin operators to **H** and **G**, and **I** is an identity operator on $\ell_2(N)$. The elementary wavelet decomposition/reconstruction step (shown in Fig. 1) results in *cA* (approximation coefficients) and *cD* (detail coefficients) sequences corresponding to a low and high frequency content of signal, respectively.

Since the decomposition step can be iterated many times (say, *J*), the discrete wavelet transformation (DWT) of *f* is an $\ell_2(N)$ sequence

$$\beta = \big(Gf, GHf, \ldots, GH^{J-1}f, H^J f\big) = \big(cD_1, cD_2, \ldots, cD_J, cA_J\big)$$

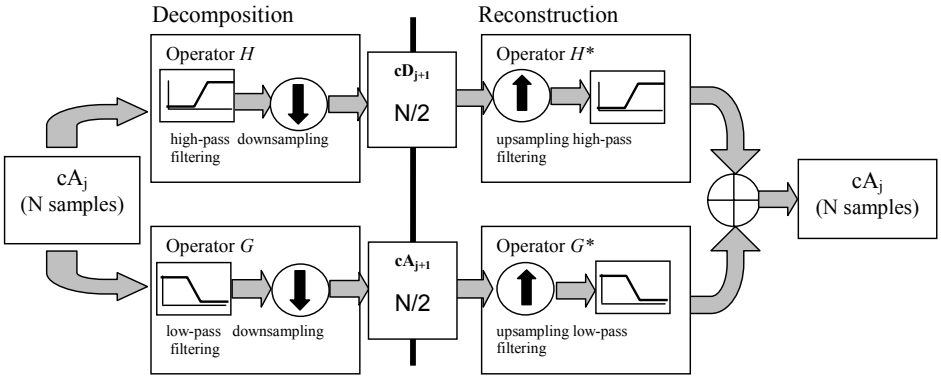

Fig. 1. Wavelet decomposition/reconstruction step

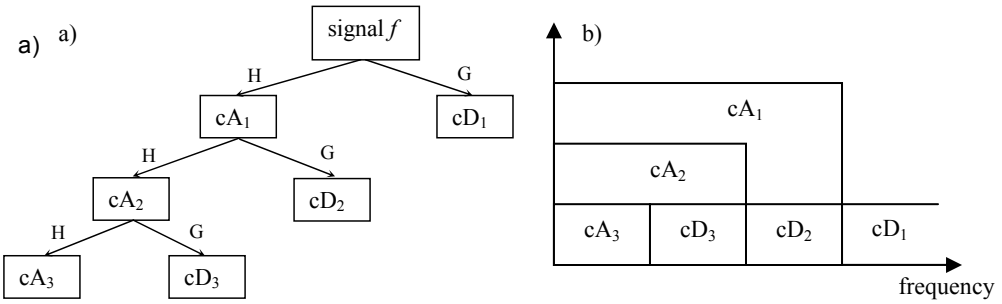

Fig. 2. Decomposition tree (DWT at level 3) (a) and frequency contents of coefficients (b)

The multi-level decomposition process (referred to as decomposition tree) is shown in Fig. 2a. Figure 2b shows the frequency content of the wavelet coefficients at different decomposition levels.

2.2. Wavelet shrinkage

The wavelet shrinkage methods achieve asymptotically near optimal minimax mean-square error for a wide range of signals corrupted by an additive white Gaussian noise. The methods derive from the basic idea that the energy of a signal (with some smoothness) will often be concentrated in a few coefficients in wavelet domain while the energy of noise is spread among all coefficients in wavelet domain. Therefore, the nonlinear shrinkage function in wavelet domain will tend to keep a few larger coefficients representing the signal while the noise coefficients will tend to reduce to zero.

The wavelet shrinkage can be described as three-step procedure:

1. A noisy signal is transformed to the wavelet domain by DWT.
2. The coefficients representing details (cD_1, ..., cD_J) are shrunk.
3. The shrunk wavelet coefficients are returned to the time domain by the inverse DWT. The result is a wavelet shrinkage estimator of the denoised signal.

Donoho et al. [3] showed that in estimating denoised signals simple shrinkage rules have asymptotic optimality properties for a rich class of function spaces. Examples are hard and soft thresholding rules, given by

$$\delta^{\text{hard}}(x,\lambda) = x \cdot 1(|x| > \lambda) \tag{1}$$

$$\delta^{\text{soft}}(x,\lambda) = (x - \text{sign}\ (x)\lambda) \cdot 1(|x| > \lambda) \tag{2}$$

where λ is a threshold parameter and $1(\cdot)$ is an indicator function.

For a fixed shrinkage policy, the parameters of shrinkage (eg. threshold λ) can be selected in many ways. The method of selecting threshold λ in soft thresholding rule (2) proposed by Donoho et al. [3] has a form:

$$\lambda = \frac{\hat{\delta}}{\sqrt{n}}\sqrt{2\log n} \tag{3}$$

where $\hat{\delta}$ is the estimator of standard deviation of details coefficients, and n is the number of details coefficients.

2.3. Wavelet shrinkage basing approach to denoising X-ray images

In our approach to noise suppression in X-ray high-resolution images we use the wavelet decomposition described in section 2.1. The decomposition level J is dependent on the number of samples in the denoised signal (N); we apply $J = 3$ for $N \approx 600$ and $J = 5$ for $N \approx 2000$. The chosen family of wavelet basis functions (determining the quadrature mirror filters) is dependent on the appearance of noisy signal, e.g. smoothness, discontinuities. We make use of Daubechies, Coifmann and Symlet wavelets families. A detailed information about families of filters can be found in [6].

The noise suppression is based on hard-thresholding rule (1). Since the method (3) of selecting the shrinkage threshold λ tends to underfit the signal (the threshold λ is too high and it shrinks too many details coefficients), we empirically found a rule for setting the threshold, which is a modification of (3):

$$\lambda = \frac{\hat{\delta}}{n}\sqrt{2\log n} \tag{4}$$

3. Experimental

Two kinds of samples were investigated:

- AlN buffer layers deposited on sapphire substrates in manufacturing high quality nitride semiconductors (e.g. GaN, (Al,Ga)N, (In,Ga)N) (the lattice mismatch in AlN/sapphire structures is about 16%). The AlN layers were deposited by the two-step pressure MOCVD process [7].

• Quantum wells (QW) based on $In_xGa_{1-x}As/GaAs$ structures deposited by the MOVPE process (lattice mismatch in such structures quickly increases with indium content and reaches 15% for InAs/GaAs structure).

A high resolution Philips diffractometer, equipped with four Ge crystal bounce Bartels monochromator in the incident beam optics and two Ge crystal bounce analyzers (RSM measurement) or receiving slit (RC measurement) in the diffracted beam optics was used for data collecting. $Cu_{K\alpha 1}$ radiation was applied. Rocking curves as well as reciprocal space maps were analyzed.

4. Results

AlN buffer layer deposited on the sapphire substrate was examined as a first example. Figure 3 shows the SEM picture of the layer cross-section parallel to the [0001] direction. The thickness observed of the AlN buffer is about 600 nm.

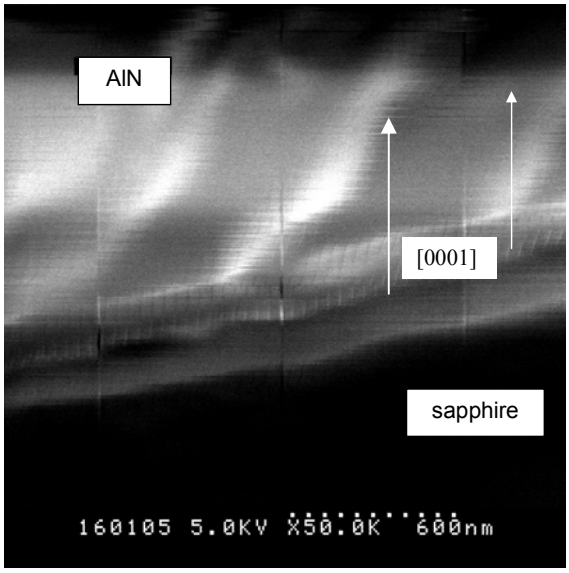

Fig. 3. SEM image of AlN buffer layer recorded perpendicular to the [0001] axis

For the same structure, the (00.2) reciprocal space map was measured. Before applying the wavelet shrinkage, a very noisy image is visible (Fig. 4a). It is obtained in a relatively short period of time (0.2 sec/step). Thanks to the wavelet analysis it was possible to extract an additional information about the examined structure from the measured map. Figure 4b shows the same map after the wavelet analysis. We can find here the thickness fringes as well as the gradient of the parameter *c* which is connected with a streak along 2theta/omega axis. The thickness of the layer, calculated from Eq. (5) [8], is equal to 608 nm ($\Delta\theta = 0.0075°$).

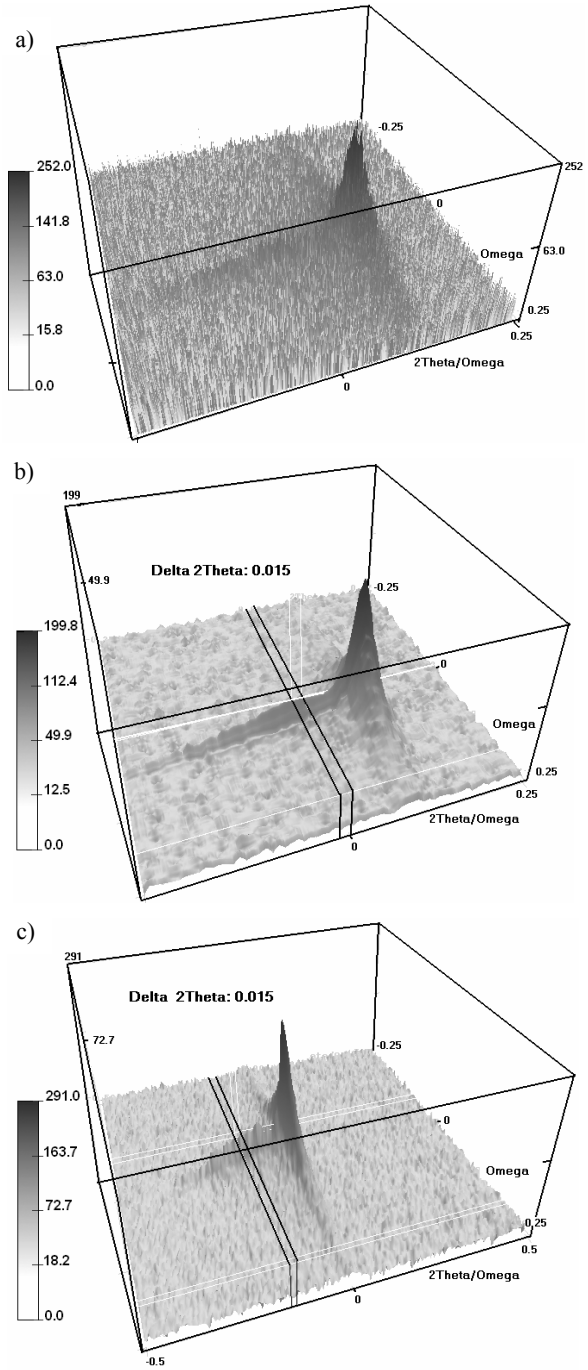

Fig. 4. (00.2) reciprocal space maps of AlN buffer layer deposited on sapphire substrate: a) measured in short time per step – 0.2 sec; b) map (a) after wavelet analysis (Daubechies wavelet (level 3)); c) measured in long time per step – 2.85 sec

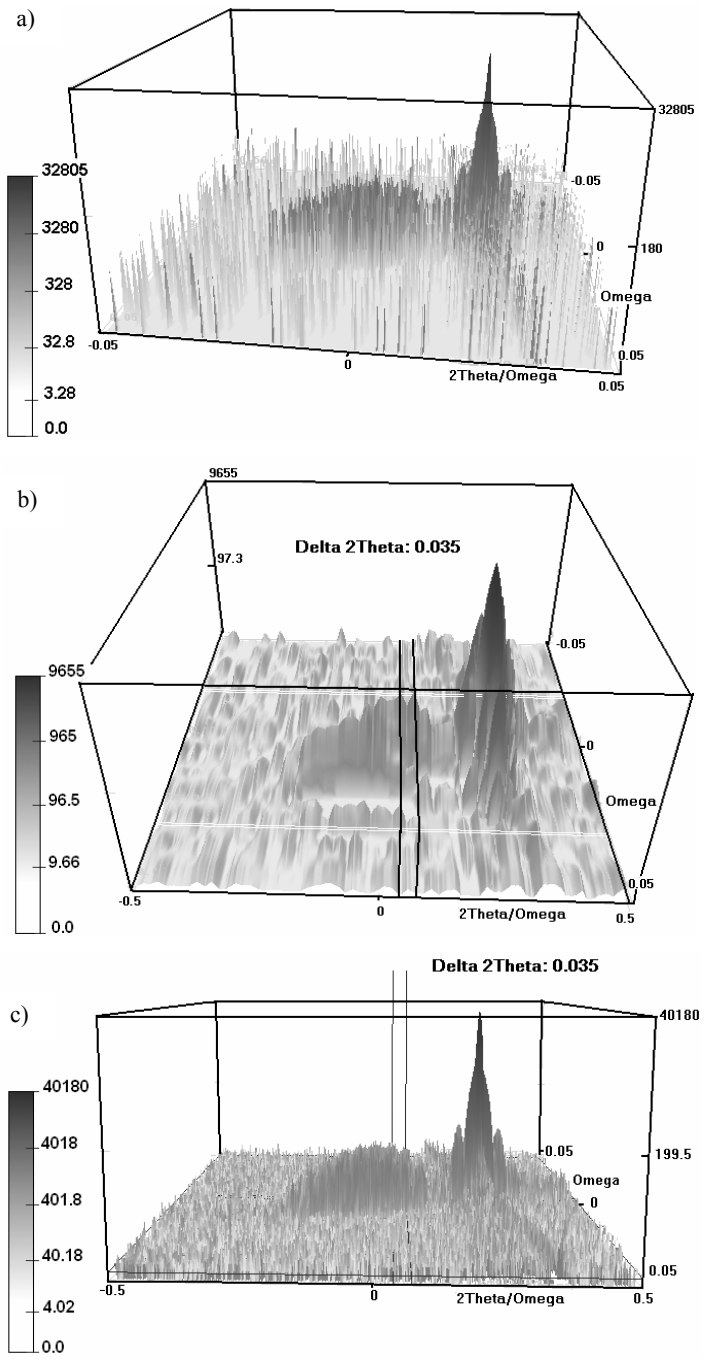

Fig. 5. (004) reciprocal space maps of quantum well GaAs/In_xGa_{1-x} As/GaAs: a) measured in short time per step – 0.05 sec; b) after wavelet analysis Symlet wavelet (level 3); c) measured in long time per step – 1.05 sec

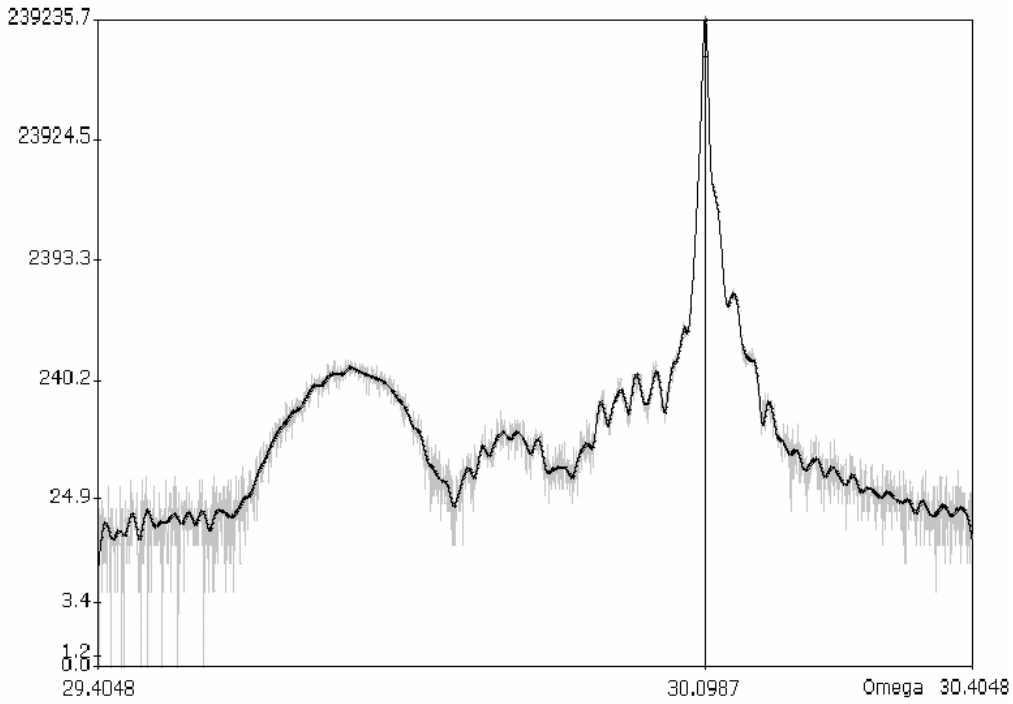

Fig. 6. Rocking curves of quantum well of GaAs/$In_xGa_{1-x}As$/GaAs (x = 0.083) measured (grey line) and after wavelet analysis (black line)

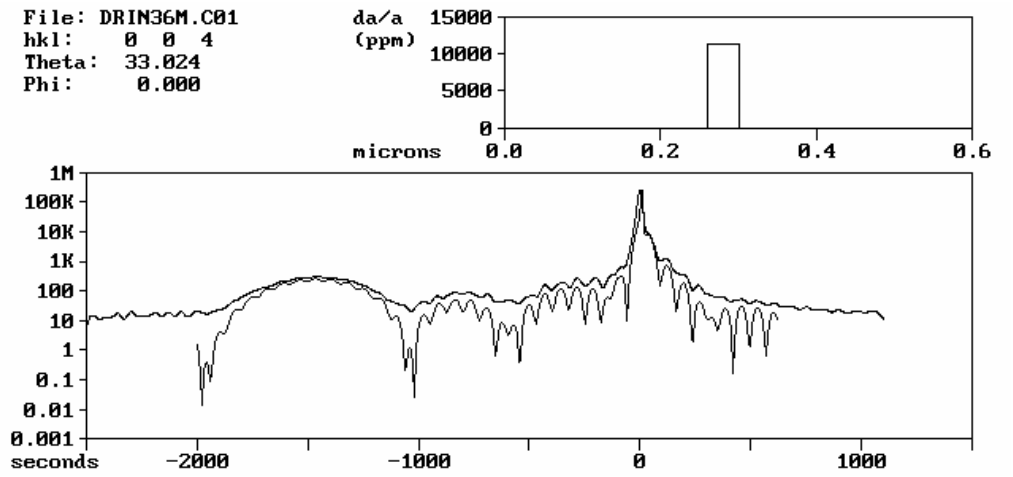

Fig. 7. Rocking curves of quantum well GaAs/$In_xGa_{1-x}As$/GaAs (x = 0.083) calculated (lower line) and after wavelet analysis (upper line)

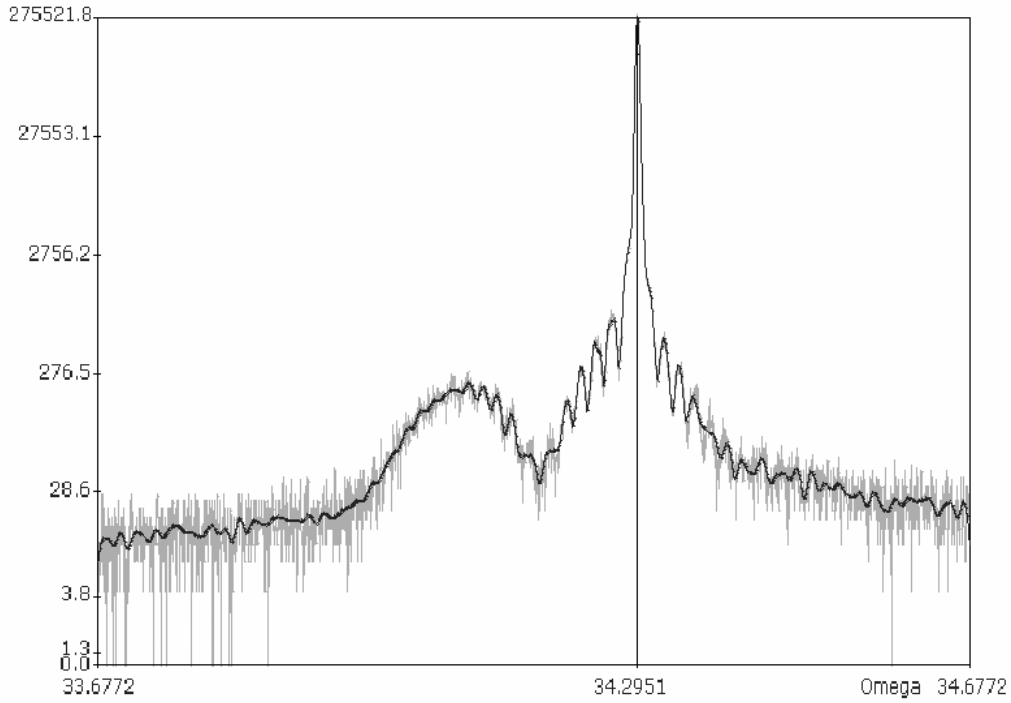

Fig. 8. Rocking curves of quantum well of GaAs/$In_xGa_{1-x}As$/GaAs (x = 0.0445) measured (grey line) and after wavelet analysis (black line)

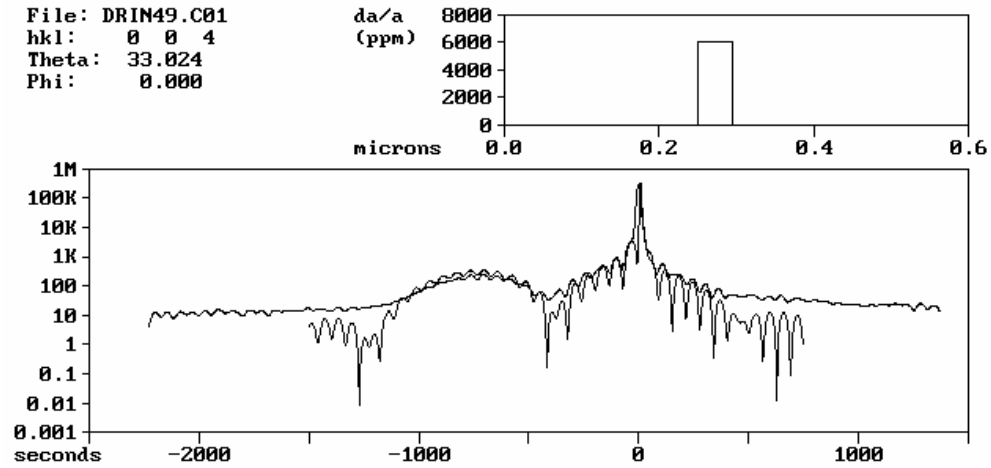

Fig. 9. Rocking curves of quantum well of GaAs/$In_xGa_{1-x}As$/GaAs (x = 0.0445) calculated (lower line) and after wavelet analysis (upper line)

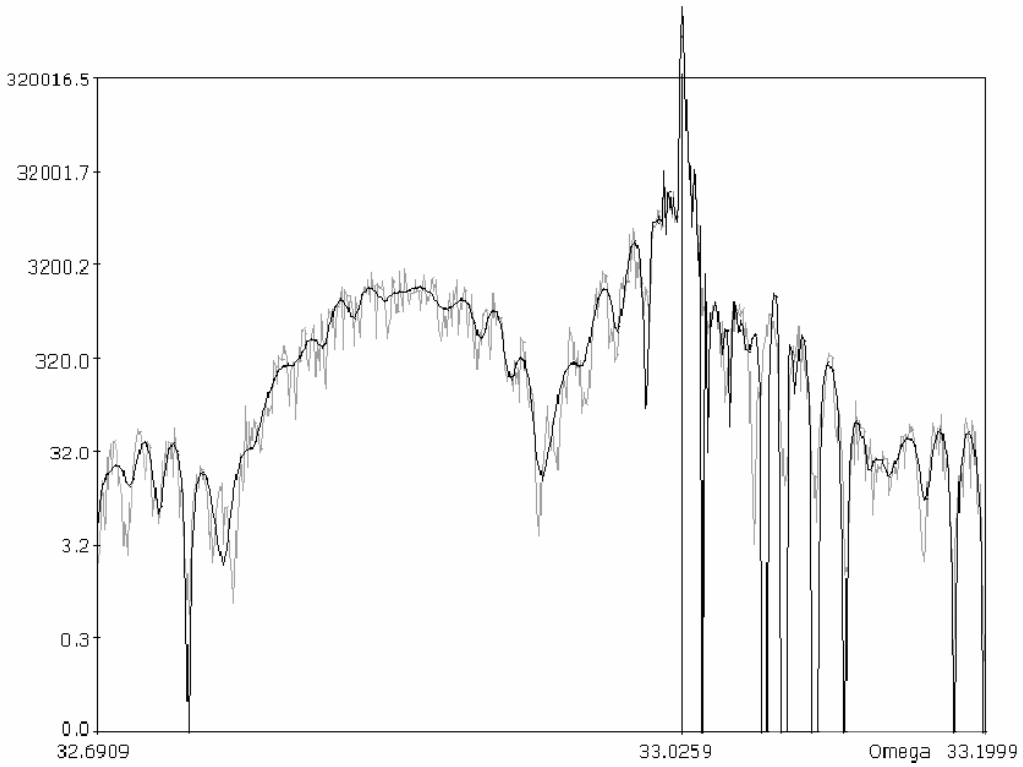

Fig. 10. Rocking curves of quantum well of GaAs/$In_xGa_{1-x}As$/GaAs (x = 0.034) randomly noised (grey line) and the same curve after wavelet analysis (black line)

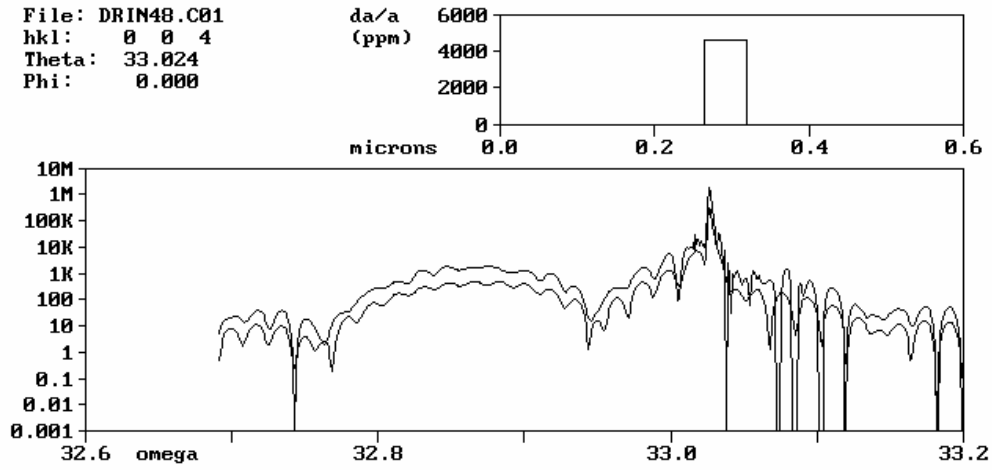

Fig. 11. Rocking curves of quantum well of GaAs/$In_xGa_{1-x}As$/GaAs (x = 0.034) calculated (lower line) and denoised after wavelet analysis (upper line)

$$t = \frac{\lambda \sin \varepsilon}{\Delta\theta \sin 2\theta} \tag{5}$$

where: t – thickness of the layer [Å], λ – X-ray wavelength [Å], ε – angle between the diffracted beam and the wafer surface [rad], θ – Bragg angle of the used reflection, $\Delta\theta$ – angle space between neighbouring fringes [rad].

Similar information can be obtained after a much longer time of scan (Fig. 4c) (2.85 sec/step). Additionally, the picture obtained from the SEM (Fig. 3) confirms the calculated thickness of the AlN buffer layer.

The next structure tested (QW) was examined on the basis of (004) RSM. Figure 5 shows the maps obtained in 1 h, 1 h after wavelet analysis and measured for 15 h. This example once again proves that it is possible to save time of measurements when the wavelet shrinkage based noise reduction is used. The details which can be observed in the denoised images are exactly the same as those in the long-time scan. The distance between the nearest interference peaks in both cases (Fig. 5b, c) is equal to 0.035° in 2 theta scale.

Figures 6–9 show the rocking curves obtained for quantum wells of GaAs (0.26 μm)/$In_xGa_{1-x}As$ (0.0421 μm, x = 0.083)/GaAs (0.235 μm) and GaAs (0.25 μm) /$In_xGa_{1-x}As$ (0.045 μm, x=0.044) /GaAs (0.277 μm), respectively. It can be seen that after the denoising procedure many more details appear which are confirmed by the theoretical calculations realized using the Takagi–Taupin equations (Figs. 7, 9).

Finally, the procedure described above was employed to denoise simulated curves obtained by superimposing a noise from a random generator onto theoretical rocking curves (Fig. 10) and the curve obtained was compared with the input curve (Fig. 11). The test also confirmed that the proposed denoising method gives credible information.

5. Conclusions

The wavelet transform was applied to the analysis of epitaxial layers of high resolution X-ray diffraction images. Rocking curves as well as reciprocal space maps were examined using the method described. It has been shown that the transformed X-ray image yields much more information about the crystallographic structure, than raw picture obtained directly from the measurements. E.g. thickness of the layer, gradient of the lattice parameters and theirs discontinuities can be obtained in this way. Particularly, the method proposed seems to be promising for the layers having large lattice mismatch with respect to substrate. All maps were visualized using OpenGL Technology. The method proposed allows a significant saving the time of measurements.

References

[1] DAUBECHIES I., Commun. Pure Appl. Math., 41 (1988), 909.
[2] MALLAT S., IEEE Trans. Pattern Anal. Machine Intel., 11 (1989), 674.

[3] DONOHO D., JOHNSTONE I., Biometrica, 91 (1994), 429.
[4] DAUBECHIES I., *Ten Lectures on Wavelets*, SIAM, Philadelphia, 1992.
[5] NASON G., *Choice of the threshold parameter in wavelet function estimation*, [in:] A. Antoniadis and G. Oppenheim (Eds.), *Wavelets and statistics,* Lecture Notes in Statistics 103, Springer, New York, 1995, p. 261.
[6] MISITI M., MISITI Y., OPPENHEIM G., POGGI J.M., *Wavelet Toolbox User's Guide*, The MathWorks Inc., Natick, 1996.
[7] PADUANO Q., WEYBURNE D., Jpn. J. Appl. Phys., 42 (2003), 1.
[8] FEWSTER P.F., Semicond. Sci. Technol., 8 (1993), 1915.

Received 28 June 2003
Revised 24 August 2003